

Semi-Supervised Active Learning for COVID-19 Lung Ultrasound Multi-symptom Classification

1st Lei Liu, 1st Wentao Lei,
3th Xiang Wan, 4th Li Liu*

Shenzhen Research Institute of Big Data
the Chinese University of Hong Kong, Shenzhen
Shenzhen, China
{220019056,220019019}@link.cuhk.edu.cn,
wanxiang@sribd.cn, liuli@cuhk.edu.cn

1st Yongfang Luo, 2nd Cheng Feng
Department of Medical Ultrasonics,

National Clinical Research Center for Infectious Disease
Shenzhen Third People's Hospital (Second Hospital Affiliated
to Southern University of Science and Technology)
Shenzhen, China
luoyongfang2005@foxmail.com, chaosheng-01@szsy.sustech.edu.cn

Abstract—Ultrasound (US) is a non-invasive yet effective medical diagnostic imaging technique for the COVID-19 global pandemic. However, due to complex feature behaviors and expensive annotations of US images, it is difficult to apply Artificial Intelligence (AI) assisting approaches for lung's multi-symptom (multi-label) classification. To overcome these difficulties, we propose a novel semi-supervised Two-Stream Active Learning (TSAL) method to model complicated features and reduce labeling costs in an iterative procedure. The core component of TSAL is the multi-label learning mechanism, in which label correlations information is used to design multi-label margin (MLM) strategy and confidence validation for automatically selecting informative samples and confident labels. On this basis, a multi-symptom multi-label (MSML) classification network is proposed to learn discriminative features of lung symptoms, and a human-machine interaction is exploited to confirm the final annotations that are used to fine-tune MSML with progressively labeled data. Moreover, a novel lung US dataset named COVID19-LUSMS is built, currently containing 71 clinical patients with 6,836 images sampled from 678 videos. Experimental evaluations show that TSAL using only 20% data can achieve superior performance to the baseline and the state-of-the-art. Qualitatively, visualization of both attention map and sample distribution confirms the good consistency with the clinic knowledge.

Index Terms—COVID-19, Ultrasound Imaging, Multi-Label Classification, Active Learning, Semi-Supervised Learning

I. INTRODUCTION

The novel coronavirus (COVID-19) has spread worldwide and is now officially a global pandemic. Typical diagnosing tools mainly include Computed tomography (CT) and X-ray, which are characterized by their relatively accurate performances [1]. However, due to the prevalence of COVID-19, in practice, deep learning-based CT or X-ray approaches remain several challenges. Firstly, CT and X-ray tools are generally time-consuming and inflexible, and involve extra radiations. Secondly, their images of COVID-19 patients are not easy to collect because their imaging procedures involve isolating patients, operating complex clinical equipment, and many other nontrivial processes.

In contrast, lung ultrasound (US) imaging is preferred as a mature tool for its fast, flexible, and reliable deployment,

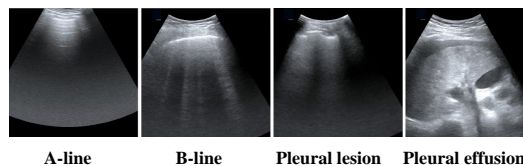


Fig. 1. Symptoms of the established COVID19-LUSMS dataset.

especially in emergencies [2]. More importantly, it is non-invasive and can work at the bedside. Recently, some works [3]–[5] focused on COVID-19 symptom detection based on lung US images. Indeed, based on lung US images, automatic AI assisting approaches for COVID-19 symptoms classification can also make significant sense for medical diagnoses of doctors. Therefore, we focus on lung ultrasound multi-symptom classification in this work.

In practice, the automatic classification of COVID-19 lung symptoms is difficult for twofold reasons. Firstly, the lung US images of COVID-19 patients may simultaneously involve multiple symptoms, which may exhibit complicated features (see in Fig. 1). One possible solution is following the multi-label learning, which targets to judge whether an image possesses multiple characteristics denoted by labels [6], [7]. Besides, it is expensive and tedious to collect and annotate numerous COVID-19 Lung US images. To address this difficulty, the feasible solution is active learning algorithm [8], [9], which aims to achieve effective performance given a limited labeling cost.

To achieve effective performance with the least labeling cost, we propose a novel semi-supervised Two-Stream Active Learning (TSAL) model, which works in an iterative procedure by a sample selection, pseudo-label validation, human-machine interaction (HMI) and CNN parameters updating alternately. In TSAL, a multi-symptom multi-label (MSML) classification network is constructed as the basic model for feature learning. Based on the label correlation information, the sample stream works for informative sample selection by newly designed multi-label margin strategy (MLM), while the label stream is exploited to assign confident pseudo-label for selected images. Then the HMI is used for confirming the

* Corresponding author

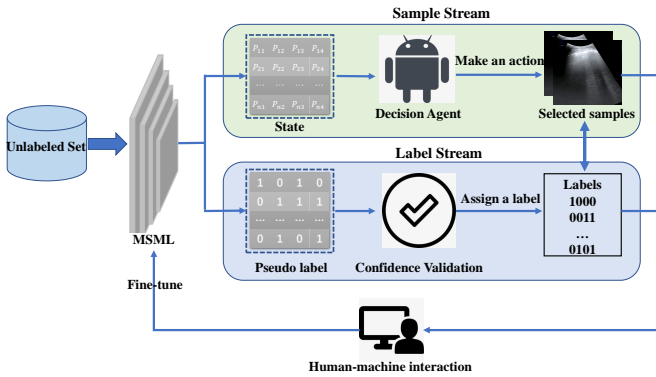


Fig. 2. Overview of the proposed framework of MSML-TSAL. Sample stream is to select informative samples by state and decision agent, which are used to describe the prediction results of all unlabeled images and determine which image candidate will be selected. Label stream is to validate and assign pseudo labels for the selected images. Human-machine interaction is to confirm the final annotations for fine-tuning MSML model. This iterative process terminates when it reaches the annotation budget or required performance.

final annotations to fine-tune the MSML. An overview of the proposed method is shown in Fig. 2.

Besides, a large-scale dataset of lung US images for COVID-19 is built for this work. Some examples are shown in Fig. 1. Experiments on this dataset show that our proposed method achieves superior classification performance, outperforming the baseline models and the state-of-the-art (SOTA) using less than 20% of the labeled images. To the best of our knowledge, this is the first work on automatic multi-symptom multi-label classification for COVID-19 lung US images.

In summary, this work contains the following three contributions:

- 1) A novel large-scale dataset containing lung US images of COVID-19 is built specifically for this work. This dataset is annotated in the multi-label form by medical experts.
- 2) We propose a novel semi-supervised TSAL method, which effectively reduces the labeling cost. It exploits label correlations information to select informative samples and confident pseudo labels.
- 3) Experimental results show that our method achieves superior performance using less than 20% labeled data, compared with baseline and SOTA. Explainable analyses using attention map and sample distribution well confirm that our results are well consistent with clinic expertise.

II. RELATED WORK

A. Lung US techniques for COVID-19

Many studies [2], [10], [11] reported the superiority of US imaging in diagnosing pneumonia and related lung conditions. Sloun *et al.* [12] proposed a fully convolutional neural network to identify and localize the B-lines in clinical lung ultrasonography. Born *et al.* [3] trained a POCOVID-Net on a 3-class dataset and achieved good accuracy in classification. The work [13] presented a novel network that simultaneously predicted the disease severity score associated with an input frame. However, they generally require a large-scale labeled US-image dataset, where annotations are expensive.

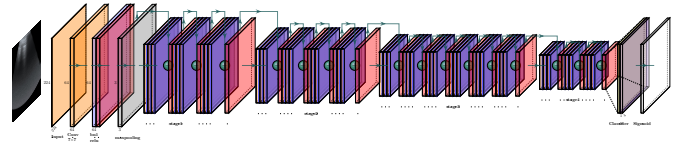


Fig. 3. Overview of the MSML model's architecture.

B. Multi-label image classification

As an important branch of classification, multi-label classification [14], [15] has been widely explored in recent years, supported by CNNs [16], [17]. Multi-label image classification plays an important part in bridging the gap between low-level features and high-level semantic information [6]. Recently, some multi-label classification methods applied CNNs for competitive performances. For a classical example, [18] optimizes top-k ranking objectives combined with convolutional architectures to learn a better feature representation. Hypotheses-CNN-Pooling [19] incorporates object segmentation hypotheses with max pooling to generate multi-label predictions. For lung US images, a COVID-19 patient may perform multiple symptoms at the same time. Thus, COVID-19 symptoms classification can be formulated as a multi-symptom multi-label classification task.

C. Active learning

AL has been successfully deployed into semantic segmentation [20]), image classification [21]), human pose estimation [8], *etc.* These applications indicate that AL is a great choice for labeling efforts reduction. Besides, there have been many popular selection strategies in the literature, mainly including query by committee, expected error reduction, expected model change, and uncertainty sampling. These strategies are usually exploited for single-label classification tasks, which is not suitable for COVID-19 lung US images classification with complex multi-label feature behaviors. In this work, to reduce the labeled cost for COVID-19 diagnosis, we introduce TSAL into multi-symptom multi-label classification to actively select informative images for annotations.

III. METHODOLOGY

A. Multi-symptom multi-label model

We propose a MSML network to tackle the COVID-19 lung US classification task, as shown in Fig. 3. Backbone is ResNet50 [16] with ImageNet pre-train for its competitive performance. The hidden FC layer is removed, while layers after the final convolutional layer are also removed to avoid too deep or too complicated architecture. Then it is followed by one specifically designed classifier consisting of average pooling and FC layer. Sigmoid cross-entropy loss is adopted to learn the discriminative features, which is defined as:

$$L_{cross} = -\frac{1}{N} \sum_{i=1}^N (y \times (\log \hat{x}) + (1 - y) \times (\log(1 - \hat{x}))), \quad (1)$$

where x is the output vector before sigmoid activation on the ground truth class y of the input image, N is the batch size, and $\hat{x} = 1/1 + e^{-x}$.

B. Two-stream deep active learning framework

The detailed framework of MSML-TSAL is presented in Fig. 2, which contains a sample stream and a label stream. The core of sample stream is to select informative samples. The label stream is to assign pseudo labels by confidence validation. At first, we perceive all unlabeled images as the candidate pool. At discrete AL iteration t , for each unlabeled image, MSML provides a prediction state S_t . Then decision agent can make an action for sample selection according to S_t and selection strategy. Then pseudo labels are assigned by confidence validation. The final annotations would be confirmed by human-machine interaction (HMI) to fine-tune the MSML model. This iterative operation repeats until the expected performance of MSML or the empty candidate pool.

1) *Sample stream: Action*: The action is to select unlabeled images from the candidate pool. The pre-defined annotation efforts for each AL iteration are denoted by K_{max} , which restricts the maximal annotation efforts for the entire MSML-TSAL. At each iteration t with the state S_t , the decision agent makes an action to select images based on the decision function $f(A_t|S_t)$. Once $A_t = \{i_1, i_2, \dots, i_{K_{max}}\}$ is executed, the decision agent is able to query them for annotations via HMI and remove them from the candidate pool.

State: The state is utilized to describe the relationship between unlabeled images and the prediction capability of the model. Prediction probability has been widely exploited to measure the prediction capability of the model in active learning tasks by using the outputs of the MSML model. In this work, we construct a prediction probability matrix to take output probabilities as the state value. Given a candidate pool $C = \{c_1, c_2, \dots, c_s\}$, where s is the size. The i th prediction vector can be extracted and written as $p_i = \{p_{i1}, p_{i2}, \dots, p_{im}\}$, where m is the number of the labels. The state S_t at discrete AL iteration t can be denoted by these as $S_t = \{p_1, p_2, \dots, p_s\}$.

Decision Agent: The decision agent is used to measure which image is worth annotating using selection strategies. To this end, we specially design an active-learning strategy called multi-label margin (MLM), which aims to evaluate the informativeness for each unlabeled sample. For lung US images of COVID-19 patients, A-line denotes the health while others denote the disease. Besides, an image cannot exhibit A-line and other symptoms simultaneously, which is also not reasonable in medical knowledge. Intuitively, if the probability of A-line has a small margin with other symptoms, it is difficult for the model to judge whether the image is healthy or unhealthy, which may be caused by the un-learned information of this image. The MLM is defined as:

$$M_x = \left| p(l_1|x) - \max_{2 \leq i \leq N} p(l_i|x) \right|, \quad (2)$$

where $p(l_1|x)$ is the probability of input image x for A-line.

Besides, it is noticed that there are few active strategies for the multi-label multi-class classification task. We redesign the classical and common strategies of multi-class classification, including Least Confidence and Entropy [22], [23] for multi-

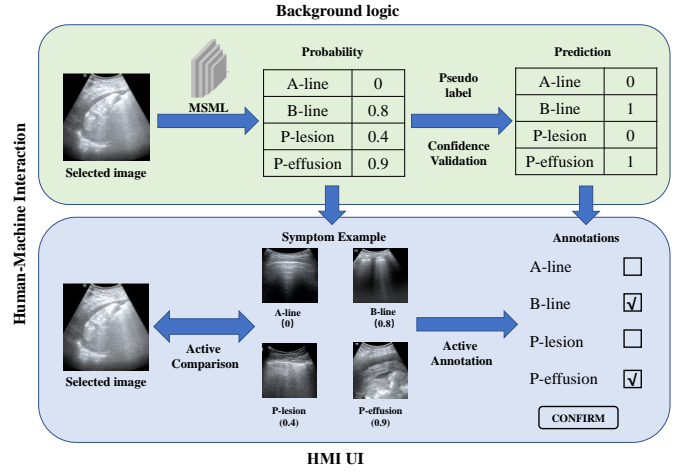


Fig. 4. Overview of the interface of human-machine interaction.

label multi-class classification. The detailed decision functions are as follows.

Least confidence (LC): lower confidence illustrates that it is a hard image for the current classifier to make a correct prediction. The calculation of LC is:

$$L_x = \min_{1 \leq x \leq M} \max_{1 \leq i \leq N} p(l_i|x), \quad (3)$$

where M is the size of the unlabeled set and N is the number of labels (*i.e.*, symptoms). $p(l_i|x)$ denotes the probability of input image x with symptom l_i .

Multi-label entropy (MLE): higher entropy indicates that the image carries rich information. The MLE is denoted as:

$$E_x = \sum_{i=1}^N (p(l_i|x) \log p(l_i|x) + p(\bar{l}_i|x) \log p(\bar{l}_i|x)), \quad (4)$$

where $p(l_i|x)$ is the probability of input image x with symptom l_i . $p(\bar{l}_i|x)$ is the probability of x that not with symptom l_i .

2) *Label stream: Pseudo label*: In the label stream, the pseudo label denotes as the most probable symptom for the input image. To this end, a fixed threshold is assigned for a pseudo label (0 or 1). For each symptom, if its prediction probability is higher than the threshold, its pseudo label is set as "1", otherwise it is "0". The final annotation is the combination of these pseudo labels for all symptoms, *i.e.*, "0101".

Confidence validation: Label correlations information has been widely employed for multi-label learning [24] by mining the potential relationships among different labels, which also can be exploited for confidence validation. In this work, we construct a label correlation table to store the intra-combination distribution information for each label combination. To construct this table, given the selected and labeled samples in AL iteration t , their prediction probabilities are denoted as a probability matrix $P^t(m, k)$, where m is the number of the labels and k is the number of the labeled samples. P^t can be divided into several submatrixes according to the label combinations of these samples, *i.e.*, $P^t \rightarrow \{P_1^t, P_2^t, \dots, P_n^t\}$,

where n is the number of the label combinations. Then we can obtain average probability vectors of these submatrixs as:

$$p_{avg}^t = average(P_i^t), i = \{1, 2, \dots, n\}. \quad (5)$$

The relationship vectors $RV = \{p_1^r, p_2^r, \dots, p_n^r\}$ can be calculated via normalization operation:

$$p_i^r = \frac{p_{avg}^i}{\sum_{j=1}^m p_{avg}^j}, i = \{1, 2, \dots, n\}, \quad (6)$$

where p_{avg}^i is the i th value of p_{avg}^i vector. Each RV vector reflects the intra-combination distribution for each label combination. Thus the label correlation table is to map from label combination to intra-combination distribution, denoted as $Tab(Com, RV)$. The table is initialized after the first AL iteration and updated in the next iterations.

Given a pseudo-label combination with its prediction probability vector \hat{p} , normalization operation is also executed to transform \hat{p} into the RSV form \hat{p}^r . The top nearest label combination in $Tab(Com, RV)$ of \hat{p}^r is defined as $Near(\hat{p}^r, Tab(Com, RV))$, which is obtained through:

$$\arg \min_{RV} Dist(\hat{p}^r, Tab(Com, RV)), \quad (7)$$

where $Dist$ is the Manhattan distance, and the distance between \hat{p}^r with each RV vector in $Tab(Com, RV)$ denotes $Dist(\hat{p}^r, Tab(Com, RV))$. $Near(\hat{p}^r, Tab(Com, RV))$ is the most confident label combination, which can be used to refine the pseudo-label combination.

After refining all pseudo-label combinations for the selected samples, a new $Tab(Com, RV)$ can be computed. To better update the table, we introduce one constraint condition to restrict the updating of $Tab(Com, RV)$. For each RV in the new $Tab(Com, RV)$, it replaces the corresponding RV in $Tab(Com, RV)$ only if it satisfies the following condition:

$$p_i^{r*} \times l_i \geq p_i^r \times l_i, i = \{1, 2, \dots, m\}, \quad (8)$$

where l_i is the i th label in the label combination.

3) *Human-machine interaction*: In this section, given the selected samples and pseudo labels, a human-machine interface is designed for the convenience of annotations. To better understand the HMI, we illustrate the interface in Fig. 4. The first row is the pipeline of pseudo-label generation, which is the background logic of the interface. The second line is the user interface, which would exhibit examples for each label and the selected image. Besides, the annotations would be made as defaults according to the pseudo label. The human annotator only needs to judge if the default annotations are consistent with the examples.

4) *CNN network updating*: MSML is updated with a fine-tuning algorithm. At each AL iteration t , the CNN is fine-tuned via selected set Set_t . During fine-tuning, only weights of the last three layers in MSML will be updated, while the remained weights will be frozen to the values from the pre-training. When more images are selected and annotated, the model becomes more robust. The renewed network is exploited upgrading the state initialization. This iterative training scheme stops with a fixed annotation budget or satisfied performance.

A. Implementation Details

We build the first version of the COVID19-LUSMS dataset, called COVID19-LUSMS v1. US videos are collected in the Third Peoples Hospital of Shenzhen, China. A total of 71 COVID-19 patients are inspected, including 678 videos. Random rotation (up to 10 degrees) and horizontal flips are used as data augmentation transformations. The SGD optimization is adopted with a learning rate as 2×10^{-3} , batch size as 32 and momentum as 0.9. K_{max} of TSAL is set as 100. The active iteration was repeated for 20 iterations at most.

B. Quantitative Analysis

1) *MSML*: The performance of the proposed MSML on the multi-symptom classification task is visualized in Fig.6, depicting the ROC curve for each label. Clearly, the model learns to classify the images, with the ROC-AUC scores of A-line, B-line and Pleural-effusion all above or equal to 0.985. While the ROC-AUC scores of Pleural-lesion is lower than other symptoms, but still more than 0.85.

In Tab. I, we illustrate the performance comparisons about two SOTA methods and four baselines including POCOVID-Net [3], NNBD [12], VGG16 [17], and ResNet [16], [16]. In detail, (1) **Accuracy**: MSML achieves the best performance with accuracy at 100%, 95.72%, and 80.98% for A-line, B-line and pleural lesion, respectively. MSML model almost outperforms all baseline models concerning accuracy. (2) **Sensitivity**: MSML model achieves 100%, 98.78%, 81.38%, and 6.08% sensitivity for A-line, B-line, pleural lesion and pleural effusion, respectively. Our MSML model performs similar sensitivity with baseline models, which is mainly because of the relatively distinct patterns. Besides, these methods perform poor sensitivity for pleural effusion. Our explanation is that multiple symptoms appearing simultaneously may cause complicated patterns, especially for pleural effusion. (3) **Specificity**: MSML model achieves 100%, 81.81%, 80.67%, and 100% specificity for A-line, B-line, pleural lesion and pleural effusion, respectively. MSML model performs best for all symptoms compared with baseline models, because the missed diagnosing cases are very few due to distinct patterns.

2) *MSML-TSAL*: We report in Tab. I the performance of MSML-TSAL with four selection strategies. (1) **Accuracy**: MLE strategy only uses 27.6% data to train an effective MSML model, whose accuracy can outperform the baseline model except for pleural effusion. MLE can use 14.7% annotated data to obtain a similar performance as the full training data. Only using 16.6% data, LC strategy can obtain comparable accuracy results as the full training set. (2) **Sensitivity**: All strategies can achieve similar sensitivity using fewer images for A-line and B-line, but perform worse for pleural lesion, because the pleural lesion is generally exhibited with other symptoms together. For pleural effusion, all strategies obtain almost 0 sensitivity when using less than 30% data, because the image number of pleural effusion is far less than others and the pleural effusion is easily influenced by the

TABLE I

COMPARISONS WITH THE BASELINES AND SOTA. THE BOLDS ARE OF OUR METHOD. LESS DATA IS BETTER AND THE HIGHER IS BETTER FOR OTHERS.

Method	A-line			B-line			P-lesion			P-effusion			data
	Acc	Sen	Spe	Acc	Sen	Spe	Acc	Sen	Spe	Acc	Sen	Spe	
VGG16	100	100	100	88.39	98.34	43.08	60.82	76.77	48.68	88.53	0	98.96	100%
ResNet34	100	100	100	90.88	96.87	63.63	73.36	81.71	67.00	89.31	0	99.84	100%
ResNet50	100	100	100	88.60	98.95	41.50	80.34	82.86	78.41	89.45	0	100	100%
ResNet101	100	100	100	90.45	98.17	55.33	79.91	82.37	78.04	89.45	0	100	100%
POCOVID-Net	100	100	100	84.97	90.35	60.47	80.84	79.90	81.55	91.02	14.86	100	100%
NNBD	100	100	100	90.31	99.91	46.64	71.86	68.20	74.65	89.45	0	100	100%
MSML+TSAL(Random)	99.85	100	100	90.74	98.52	65.61	83.47	77.92	98.87	89.38	0	99.92	16.6%
MSML+TSAL(MLE)	100	100	100	89.52	97.56	52.96	80.34	75.94	83.68	89.45	0	100	27.6%
MSML+TSAL(LC)	100	100	100	94.30	95.91	86.95	83.19	78.74	86.57	89.45	0	100	16.6%
MSML	100	100	100	95.72	98.78	81.81	80.98	81.38	80.67	90.09	6.08	100	100%
MSML+TSAL(MLM)	100	92.38	100	98.50	98.79	92.49	83.26	76.77	96.36	89.45	0	100	14.7%

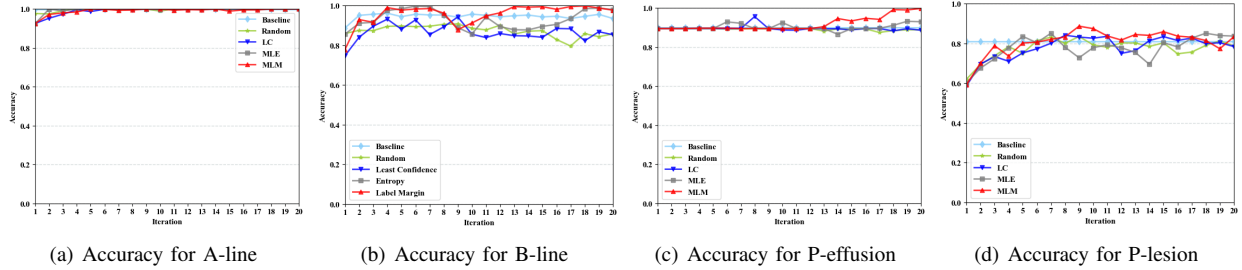


Fig. 5. Comparisons of the proposed MSML-TSAL method with different selection strategies on accuracy. Baseline means using all labeled images in the dataset without using any selection strategy. Abscissa indicates the training iterations.

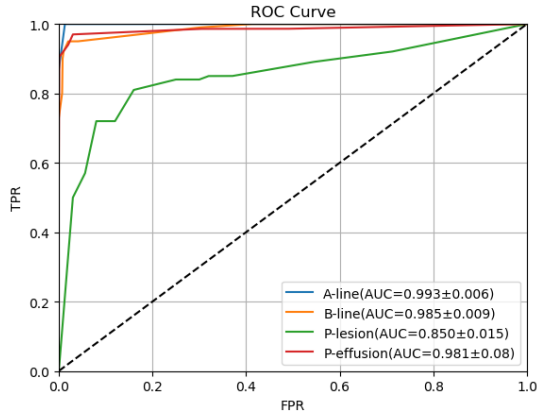
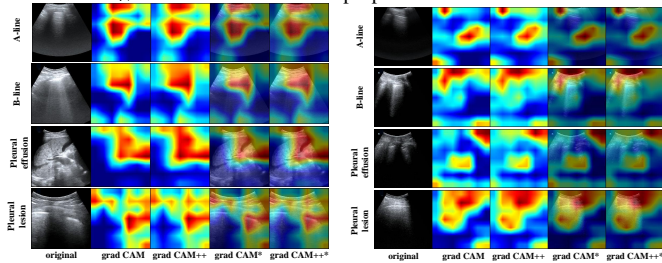


Fig. 6. ROC curve for the proposed MSML model.



(a) Test samples for MSML (b) Selected samples for MSML-TSAL

Fig. 7. Visualized results. (a) The training weights of MSML is used for visualization. (b) The training weights of MSML-TSAL is used for visualization of selected samples. (*) denotes that the attention map is overlapped on the original image.

doctor's operations. (3) **Specificity**: These strategies merely exploit 16.6%, 27.6%, 16.6%, and 14.7% data to achieve similar or better specificity performance, among which the random strategy performs worst. Surprisingly, MSML-TSAL can improve specificity for B-line and pleural effusion by a large margin, which is because that selection strategies can alleviate the unbalanced problem.

In Fig. 5, we summarize the accuracy improvement curves of MSML-TSAL combined with four selection strategies that achieve the best performance on COVID19-LUSMS dataset. Almost all curves of different strategies can achieve a similar and better performance compared with the baseline that uses the full training set (light blue curves). During the whole training process, these curves have several oscillations, indicating that features in the COVID19-LUSMS dataset are complex. Besides, we note that MLM (red curves) performs the best among the 4 strategies, with its highest accuracy at the final AL iteration. From the view of the smoothness, the MLM performs the most stable changing tendency.

C. Qualitative Analysis

1) **MSML**: As shown in Fig. 7(a), attention regions from the MSML model are consistent with the regions from the doctor. Based on clinical medical observation, A-line has an obvious horizontal-line region in the upper part of the images. B-line has an obvious vertical-line region in the whole image. Pleural effusion has many obvious irregular regions in the

TABLE II
AMOUNT OF MANUALLY LABELED DATA.

Iteration	1st	2nd	3rd	4th	5th
HMI	100%	100%	100%	100%	100%
HMI + pseudo-label	100%	29%	11%	5%	1%
HMI + pseudo-label + CV	100%	2%	1%	0%	0%

whole image. Pleural lesion has many obvious irregular lines around the pleura, which lies in the top position of the lung US image. Corresponding to the attention heatmaps, all of the visualized attention regions perform consistent results with the clinical medical observation.

2) *MSML-TSAL*: As shown in Fig. 7(b), these images contain large dark regions, which are not pathological changing regions and may cause complicated characteristics for the model learning. These characteristics are not well learned via previous training because the attention regions are likely to focus on the dark regions. Thus, these images should join in further training for their complicated information.

D. Component analysis for label stream

To justify that label stream works well for pseudo-label assignment, we conduct an ablation study for the component analysis. CV is confidence validation. As shown in Tab. II, human annotators need to manually annotate all selected images in each iteration, only using HMI without pseudo-label and confidence validation. By pseudo-label, the manual annotations gradually decrease with the performance improvement of *MSML*. Confidence validation can further reduce the manual annotations, *i.e.*, nearly zero after the first iteration. Through label stream, the selected samples can be automatically annotated, while human annotators only need to confirm annotations in HMI rather than manual annotations.

V. CONCLUSION

To achieve accurate classification of COVID-19 multiple symptoms of the lung US image with less annotated data, we innovatively propose a *TSAL* framework to effectively train the *MSML* model with less labeling efforts in a semi-supervised manner. Specifically, we design the *MLM* strategy and confidence validation for *TSAL* by label correlations information. Moreover, a novel large-scale lung US image dataset with multiple COVID-19 symptoms is built in this work. Quantitative and qualitative experimental results show that the *TSAL* model can achieve competitive performance, and we can train an effective *MSML* model merely using less than 20% data of full training set. In future work, it is worthwhile to explore the reinforcement learning to learn a powerful and adaptive policy for image selection.

REFERENCES

[1] D. Wang, B. Hu, C. Hu, F. Zhu, X. Liu, J. Zhang, B. Wang, H. Xiang, Z. Cheng, Y. Xiong *et al.*, "Clinical characteristics of 138 hospitalized patients with 2019 novel coronavirus-infected pneumonia in wuhan, china," *JAMA*, vol. 323, no. 11, pp. 1061–1069, 2020.
[2] J. E. Bourcier, S. Braga, and D. Garnier, "Lung ultrasound will soon replace chest radiography in the diagnosis of acute community-acquired pneumonia," *Current Infectious Disease Reports*, vol. 18, no. 12, pp. 1534–3146, 2016.

[3] J. Born, G. Brndle, M. Cossio, M. Disdier, J. Goulet, J. Roulin, and N. Wiedemann, "Pocovid-net: Automatic detection of covid-19 from a new lung ultrasound imaging dataset (pocus)," 2020.
[4] Y. Huang, S. Wang, Y. Liu, Y. Zhang, C. Zheng, Y. Zheng, C. Zhang, W. Min, M. Yu, and M. Hu, "A preliminary study on the ultrasonic manifestations of peripulmonary lesions of non-critical novel coronavirus pneumonia (covid-19)," 2020.
[5] Q.-Y. Peng, X.-T. Wang, and L.-N. Zhang, "Findings of lung ultrasonography of novel corona virus pneumonia during the 20192020 epidemic," *Intensive Care Medicine*, pp. 1–2, 2020.
[6] L. Li, S. Wang, S. Jiang, and Q. Huang, "Attentive recurrent neural network for weak-supervised multi-label image classification," in *Proceedings of the ACM International Conference on Multimedia*, 2018.
[7] H. Guo, X. Fan, and S. Wang, "Human attribute recognition by refining attention heat map," *Pattern Recognition Letters*, vol. 94, pp. 38–45, 2017.
[8] B. Liu and V. Ferrari, "Active learning for human pose estimation," in *IEEE International Conference on Computer Vision*, 2017.
[9] A. Vezhnevets, J. M. Buhmann, and V. Ferrari, "Active learning for semantic segmentation with expected change," in *IEEE International Conference on computer vision and pattern recognition*, 2012, pp. 3162–3169.
[10] J. E. Bourcier, J. Paquet, M. Seinger, E. Gallard, J. P. Redonnet, F. Cheddadi, D. Garnier, J. M. Bourgeois, and T. Geeraerts, "Performance comparison of lung ultrasound and chest x-ray for the diagnosis of pneumonia in the ed," *American Journal of Emergency Medicine*, vol. 32, no. 2, pp. 115–118, 2014.
[11] A. S. Claes, P. Clapuyt, R. Menten, N. Michoux, and D. Dumitriu, "Performance of chest ultrasound in pediatric pneumonia," *European Journal of Radiology*, vol. 88, no. Complete, pp. 82–87, 2017.
[12] R. J. G. Van Sloun and L. Demi, "Localizing b-lines in lung ultrasonography by weakly supervised deep learning, in-vivo results," *IEEE Journal of Biomedical and Health Informatics*, vol. 24, no. 4, pp. 957–964, 2020.
[13] S. Roy, W. Menapace, S. Oei, B. Luijten, E. Fini, C. Saltori, I. Huijben, N. Chennakeshava, F. Mento, A. Sentelli, E. Peschiera, R. Trevisan, G. Maschietto, E. Torri, R. Inchingolo, A. Smargiassi, G. Soldati, P. Rota, A. Passerini, R. J. G. Van Sloun, E. Ricci, and L. Demi, "Deep learning for classification and localization of covid-19 markers in point-of-care lung ultrasound," *IEEE Transactions on Medical Imaging*, 2020.
[14] G. Tsoumakas and I. Katakis, "Multi-label classification: An overview," *International Journal of Data Warehousing and Mining*, vol. 3, no. 3, pp. 1–13, 2009.
[15] M.-L. Zhang and Z.-H. Zhou, "A review on multi-label learning algorithms," *IEEE Transactions on Knowledge and Data Engineering*, vol. 26, pp. 1819–1837, 08 2014.
[16] K. He, X. Zhang, S. Ren, and J. Sun, "Deep residual learning for image recognition," in *IEEE International Conference on computer vision and pattern recognition*, 2016, pp. 770–778.
[17] K. Simonyan and A. Zisserman, "Very deep convolutional networks for large-scale image recognition," in *International Conference on Learning Representations*, 2015.
[18] Y. Gong, Y. Jia, T. Leung, A. Toshev, and S. Ioffe, "Deep convolutional ranking for multilabel image annotation," 2014.
[19] Y. Wei, W. Xia, J. Huang, B. Ni, J. Dong, Y. Zhao, and S. Yan, "Hcp: A flexible cnn framework for multi-label image classification," *IEEE Transactions on Pattern Analysis and Machine Intelligence*, pp. 1901–1907, 2016.
[20] Q. Sun, A. Laddha, and D. Batra, "Active learning for structured probabilistic models with histogram approximation," in *IEEE International Conference on computer vision and pattern recognition*, 2015.
[21] W. H. Beluch, T. Genewein, A. Nürnberger, and J. M. Köhler, "The power of ensembles for active learning in image classification," in *IEEE International Conference on computer vision and pattern recognition*, 2018.
[22] A. Holub, P. Perona, and M. C. Burl, "Entropy-based active learning for object recognition," in *2008 IEEE Computer Society Conference on Computer Vision and Pattern Recognition Workshops*, 2008, pp. 1–8.
[23] B. Settles, "Active learning literature survey," University of Wisconsin–Madison, Computer Sciences Technical Report 1648, 2009.
[24] M. Zhang and Z. Zhou, "A review on multi-label learning algorithms," *IEEE Transactions on Knowledge and Data Engineering*, vol. 26, no. 8, pp. 1819–1837, 2014.